Supplement of Atmos. Chem. Phys., 18, 14609–14622, 2018
https://doi.org/10.5194/acp-18-14609-2018-supplement

Atmospheric Chemistry and Physics
Open Access
EGU

Supplement of

Simulation of heterogeneous photooxidation of SO_2 and NO_x in the presence of Gobi Desert dust particles under ambient sunlight

Zechen Yu and Myoseon Jang

Correspondence to: Myoseon Jang (mjang@ufl.edu)

Section 1: Chamber experimental procedure and chamber characterization

Indoor chamber experiment

The indoor chamber experiments were performed in a 2 m^3 Teflon indoor chamber equipped with UV lamps (Wavelength: 280nm – 900 nm) (Solarc Systems Inc., FS40T12/UVB). The RH and the concentration of trace gases and dust particles were controlled to variety specific experimental conditions. During the experiment, the gases were continuously measured using a gas chromatography–flam ionization detector (HP–5890 GC–FID) for organic gases, a fluorescence TRS analyzer (Teledyne Model 102E) for SO_2, a chemiluminescence NO/NOx analyzer (Teledyne Model T201) for NO_x and a photometric ozone analyser (Model 400E, Teledyne, USA). The suspended particles were continuously measured by a scanning mobility particle sizer (SMPS, TSI 3080, USA) and an Optical Particle Counter (OPC, TSI 3330, USA). The mass concentration of inorganic iron was measured using a Particle–Into–Liquid Sampler (Applikon, ADISO 2081) combined with Ion Chromatography (Metrohm, 761 Compact IC) (PILS–IC).

Outdoor chamber experiment

The outdoor experiments were conducted using the University of Florida Atmospheric Photochemical Outdoor Reactor (UF–APHOR) dual chambers located on the roof of Black Hall at University of Florida, Gainesville, Florida (latitude/longitude: 29.64185°/-82.347883°). The total volume of the two half-cylinder shaped chamber is 52 m^3 each. The surface to volume ratio is 1.65 m^2 m^{-3} for each chamber. The chambers are built with 0.13 mm FEP Teflon film. The meteorological parameters (i.e., temperature, relative humidity, sunlight spectrum and sunlight intensity) are monitored simultaneously both inside and outside the chambers using a hygrometer (CR1000 Measurement and Control System, Campbell Scientific) (temperature and humidity), a fibro–optical portable spectrometer (EPP2000, Stellar Net Inc., USA) (sunlight spectrum) and an ultraviolet radiometer (TUVR, Eppley Laboratory Inc.). In addition, the wall loss rate constants of ozone, SO_2, H_2O_2 and HONO were measured via separate experiments. The rate constant of particle loss to the chamber wall was also measured for Arizona Test Dust (ATD) particles, Gobi Desert Dust (GDD) particles and the ammonia sulfate inorganic seeded aerosol. The typical particle distributions of ATD particles and GDD particles are shown in the Fig. S1.

Before each experiment, the dual chambers were flushed and cleaned by the air purifier system (GC Series, IQ Air Inc.). The background ion concentrations were measured every time before

experiments. Non–reactive CCL_4 (400 ppb) was injected into the dual chamber to determine the chamber dilution factor. Due to the chamber dilution, ambient trace gases (i.e., CO, O_3, CH_4, HCHO and volatile organic compounds) outside the chamber are intruded into the chamber. The estimated concentration of background gases are 1.8 ppb CH_4, 18 ppb HCHO, 6 ppb CH_3CHO, 0.1 ppb isoprene and 1 ppb HONO. The measurement procedures of gases, inorganic iron concentration and particle distribution were similar to that of indoor chamber experiments. For measuring the total particle mass concentration, the suspended particles were collected on a 13mm diameter Teflon–coated glass fiber filter (Pall Life Science Pallflex, TX40HI20–WW) for 20 minutes. The filter mass difference was measured using a microbalance (MX5, Mettler Toledo, Columbus, OH).

Section 2: Estimation of reactive uptake coefficient

The reactions of trace gases on the dust particles are traditionally expressed based on the first order reaction using the reactive uptake coefficient (γ). In AMAR model, the oxidation of trace gases in dust phase includes the 1st order and the 2nd order reactions (Table S2). Furthermore, the rate constants of heterogeneous reactions are photocatalytically and dynamically changing through day and night. For convenience, we calculate γ of SO_2 and NO_2 using the gas-dust partitioning coefficients and the rate constants as follows (Yu et al., 2017),

$$\gamma_{dark,SO_2} = \frac{4K_{d,SO_2}k_{auto,SO_2}}{\omega_{SO_2}} \quad \text{for } SO_2 \text{ autoxidation} \quad \text{(S1)}$$

$$\gamma_{light,SO_2} = \frac{4K_{d,SO_2}\left(k_{photo,SO_2}[\mathrm{OH(d)}]+k_{auto,SO_2}\right)}{\omega_{SO_2}} \quad \text{for } SO_2 \text{ photooxidation} \quad \text{(S2)}$$

$$\gamma_{dark,NO_2} = \frac{4K_{d,NO_2}k_{auto,NO_2}}{\omega_{NO_2}} \quad \text{for } NO_2 \text{ autoxidation} \quad \text{(S3)}$$

$$\gamma_{light,NO_2} = \frac{4K_{d,NO_2}\left(k_{photo,NO_2}[\mathrm{OH(d)}]+k_{auto,NO_2}\right)}{\omega_{NO_2}} \quad \text{for } NO_2 \text{ photooxidation} \quad \text{(S4)}$$

ω (m s^{-1}) is the mean molecular velocity of gas species. k_{auto} (s^{-1}) is the first order rate constant for autoxidation of SO_2 or NO_2 and k_{photo} (cm^3 $molecule^{-1}$ s^{-1}) is the second order rate constant for photooxidation of SO_2 or NO_2 by OH radicals on dust particles. [OH(d)] (molecule per cc of air) is the concentration of OH radicals on dust. K_d (m^3 m^{-2}) is the gas-dust partitioning coefficient and is calculated using the geometric surface concentration of airborne dust particles (A_{dust}, m^2 m^{-3}). K_d can be calculated as,

$$K_d = \frac{[\mathrm{gas(d)}]}{[\mathrm{gas(g)}]A_{dust}} \text{ and} \quad \text{(S5)}$$

$$K_d = \frac{k_{up}}{k_{off}}, \quad \text{(S6)}$$

where [gas(d)] and [gas(g)] are the concentration of gas species in dust and gas phase, respectively. k_{up} and k_{off} is first calculated for SO_2 and then scaled using Henry's law constant for other gaseous compounds (Yu et al., 2017). Figure S4 illustrates the time profile of γ under the ambient environmental conditions on November 23, 2017.

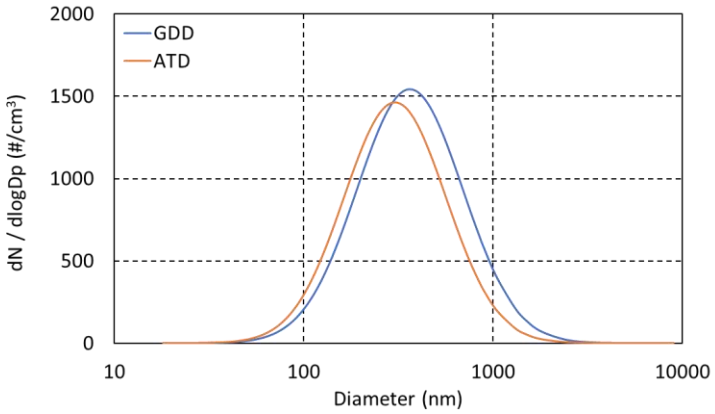

Figure S1. Particle size distribution of ATD and GDD dust samples measured during outdoor chamber experiments. The geometric surface area of ATD and GDD particles used in this study were 3.1 and 2.6 m^2 g^{-1}, respectively.

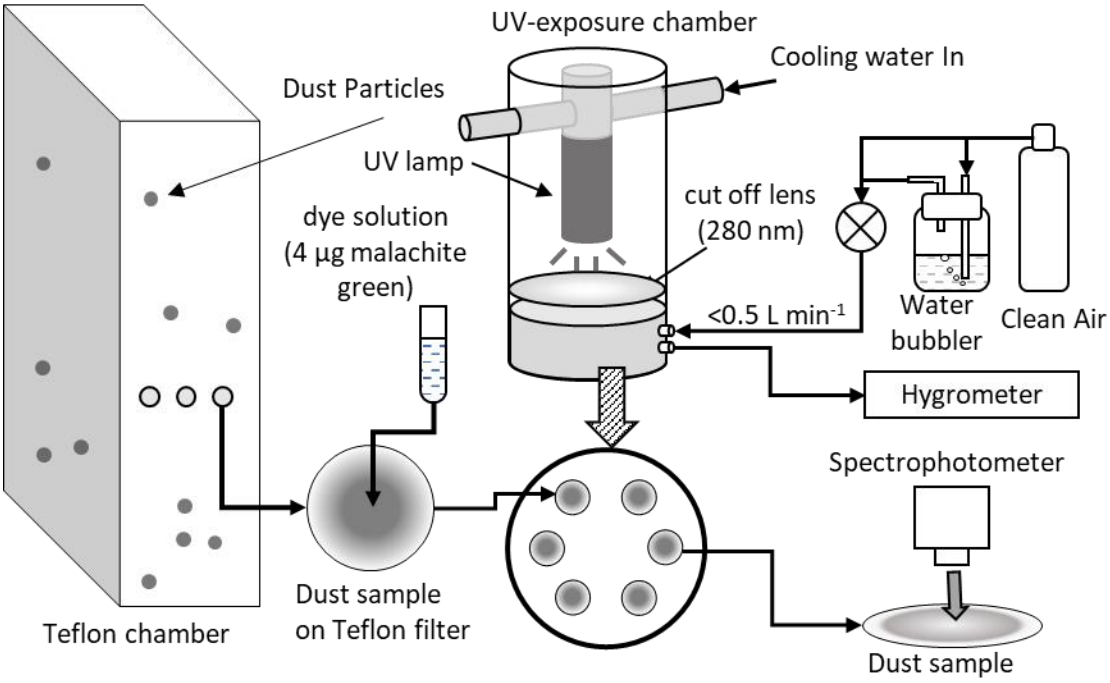

Figure S2. The experimental setup to measure the photoactivation capability of dust particles ($[M^*]_{dust}$ in Eq. (2)). The dust filter was impregnated with 4 µg malachite green using ethanol solution (0.2 g L^{-1}). The humidity inside the exposure box is controlled ranging from less than 10% to 80%.

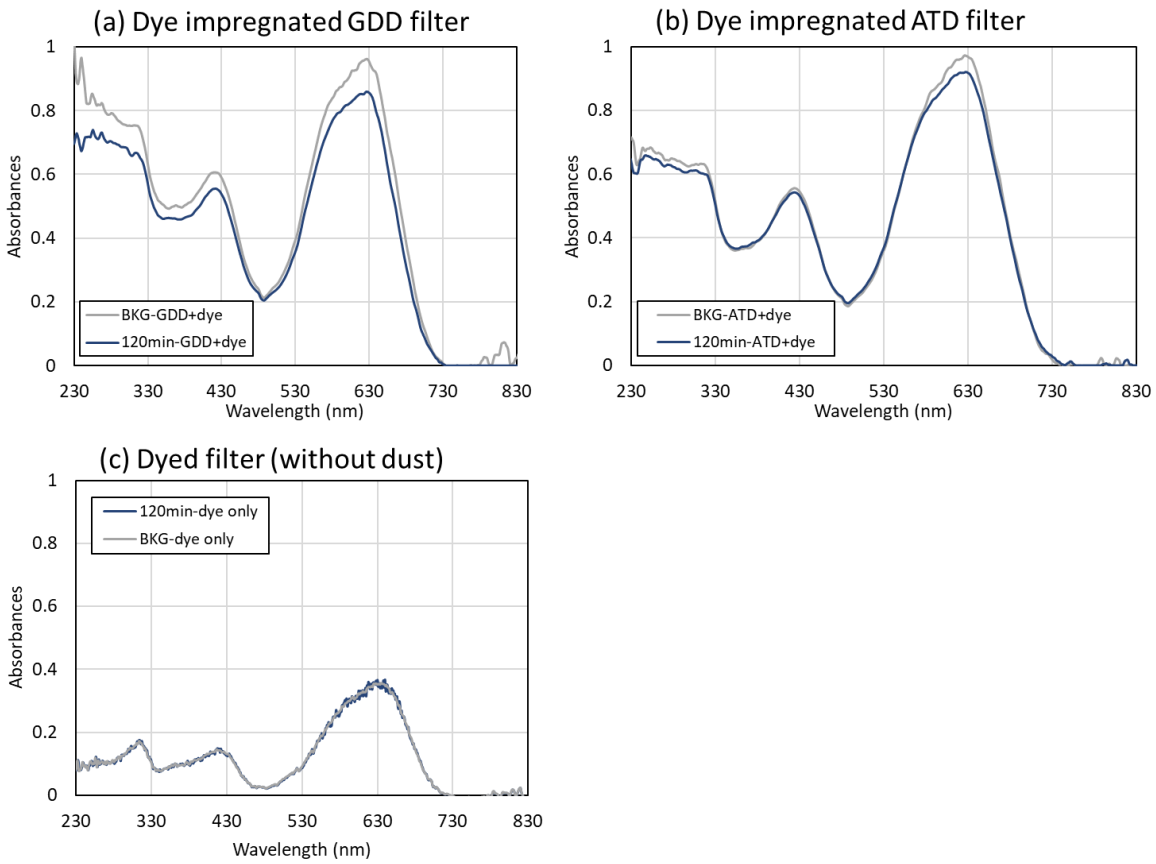

Figure S3: Light absorbance of GDD filter samples that is impregnated with malachite green dye (Fig. S2) before and after irradiation for 120 minutes using UV light (a) The light absorbance of dye impregnated GDD filter samples measured before and after irradiation for 120 minutes using UV light; (b) The light absorbance of dye impregnated ATD filter samples measured before and after irradiation for 120 minutes using UV light. The fabricated flow chamber is operated at 55% RH and the mass of the dust on the filter was 161 µg for ATD filter and 159 µg for the GDD filter. The degradation of dye in the absence of dust particles is negligible (c).

(a)

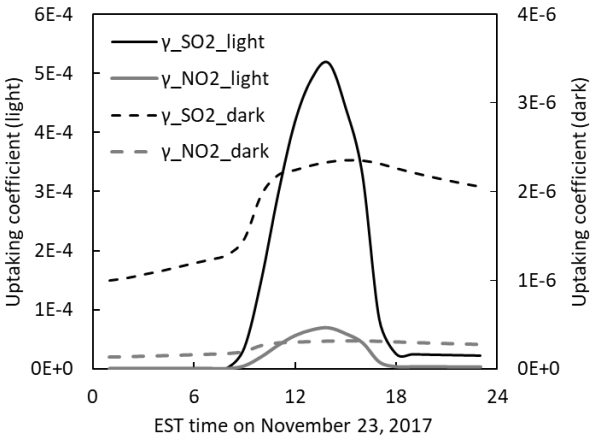

(b)

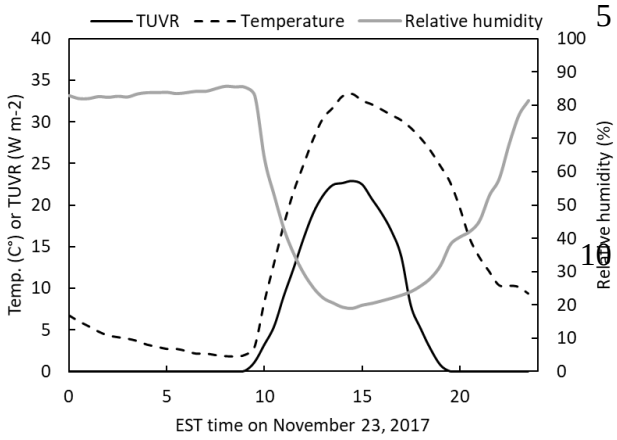

Figure S4. (a) Time profile of reactive uptake coefficient (γ) of SO_2 and NO_2 on Gobi Desert Dust particles under ambient sunlight. γ is calculated using simulation results that are conducted with 200 μg m^{-3} GDD particles, 40 ppb SO_2 and 20 ppb NO_2 under ambient conditions on 23 November 2017. The particle loss is not considered in the simulation. (b) Time profile of temperature (C°), relative humidity (%) and Total UV radiation (TUVR, W m^{-2}) on November 23, 2017 at Gainesville, Florida (latitude/longitude: 29.64185°/–82.347883°).

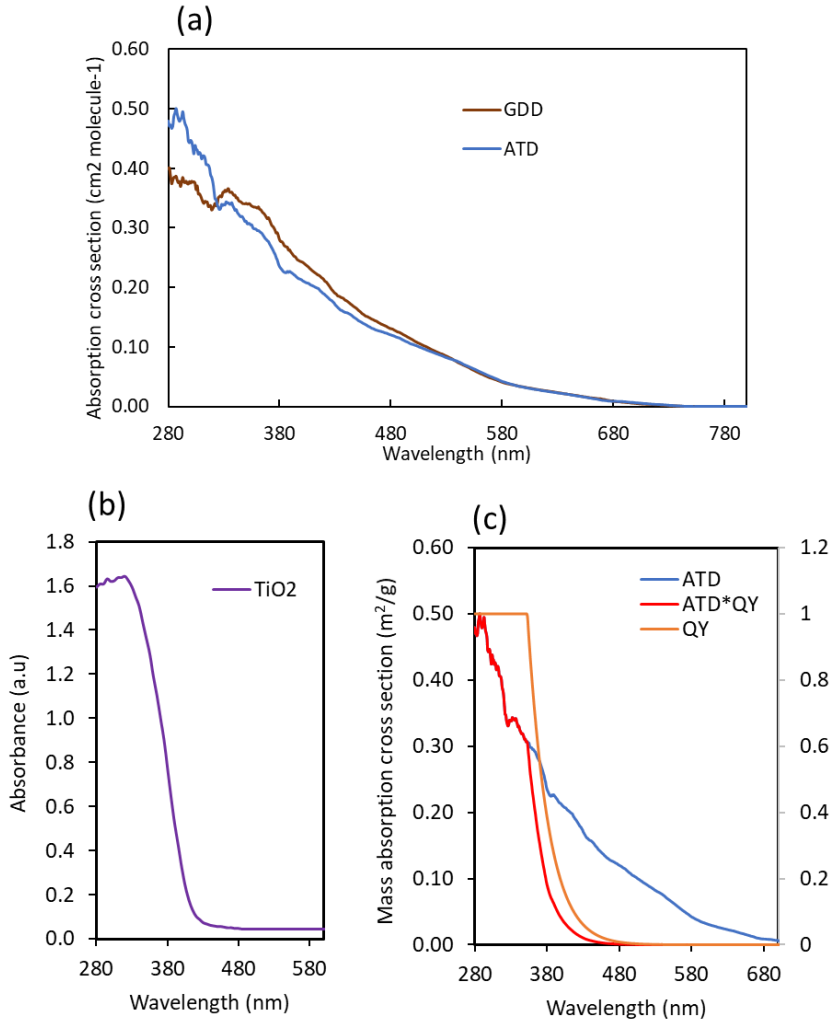

Figure S5 Light absorbance ATD and GDD (a). light absorption of TiO_2 and its integration with light absorption of dust particles and quantum yield of (b and c). The light absorbance and quantum yield of ATD are measured and reported in our recent study (Yu et al., 2017).

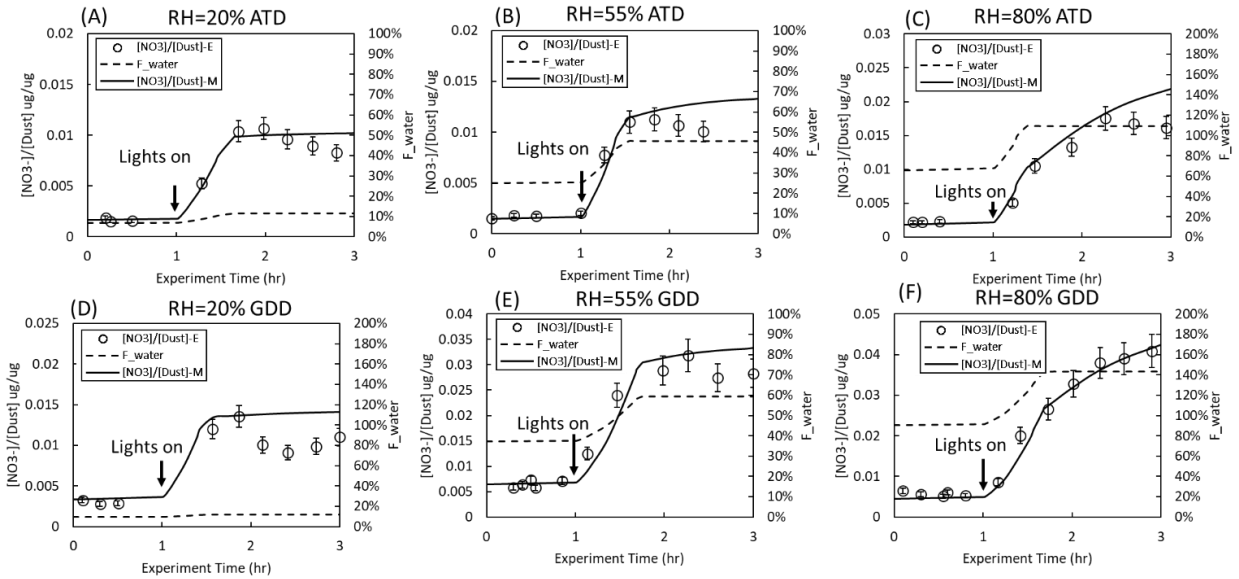

Figure S6. Measurement and simulation of nitrate formation using indoor chamber in the presence of ATD or GDD particle under the three different humidities (20%, 55% and 80%). "Exp" and "Pred" represents the experimental observations and the model predictions, respectively. The error associated with the mass fraction of nitrate on dust particles is ±10% and this originates from PILS-IC measurements. The UV light was on 1 hour after starting the experiment. The details of chamber conditions are shown in Table S1.

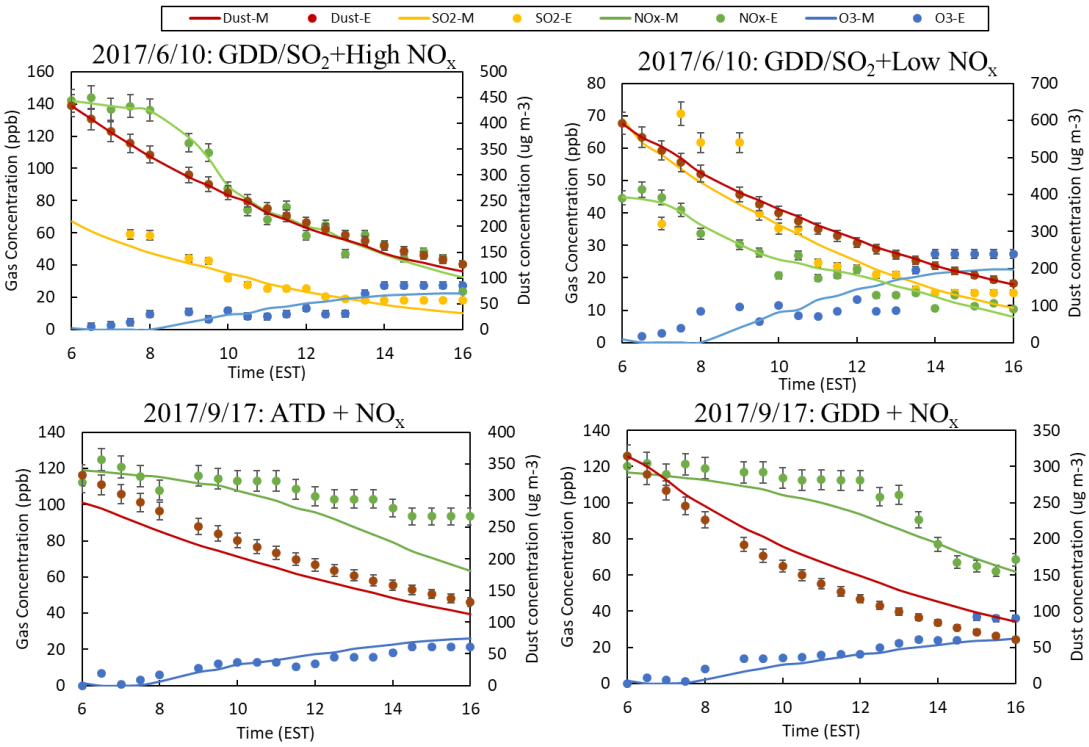

Figure S7. The time profile of concentrations of gaseous compounds and dust mass for the experiments on 2017-6-10 and 2017-9-17 (Table 1).

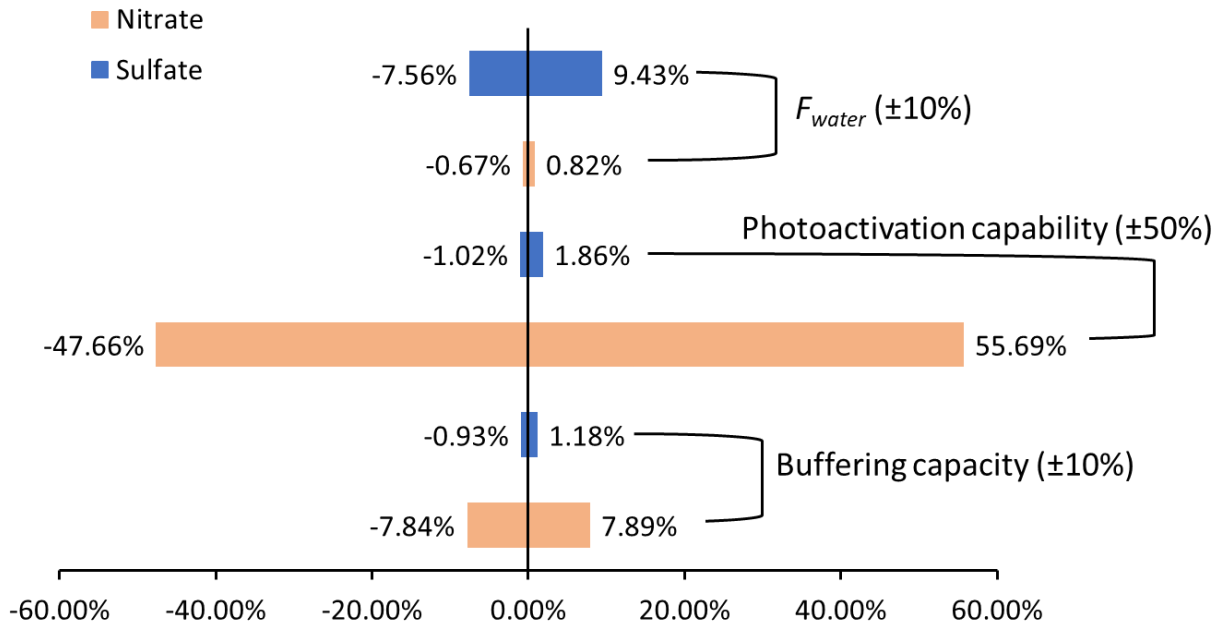

Figure S8. Uncertainties of prediction of sulfate and nitrate due to the variation of F_{water}, the photoactivation capability ($[M^*]_{dust}$ in Eq. (2)) and the buffering capacity of dust (also see Figure S7). All simulation was performed with 100 µg m^{-3} of initial GDD particles, 2 ppb of initial O_3 and 10 ppb isoprene under ambient environmental condition on 23 November 2017. For nitrate production initial 40 ppb NO_x was used and for sulfate formation 40 ppb SO_2 and 2 ppb NOx. The simulation was performed without considering the particle loss to the chamber wall.

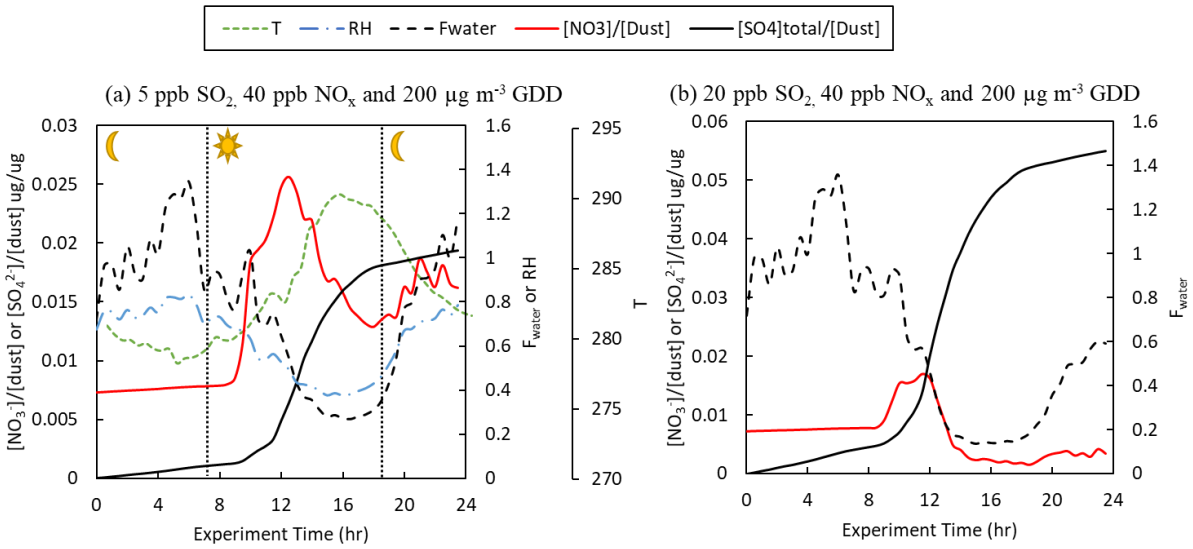

Figure S9. 24-hour simulation for the production of nitrate and sulfate using the AMAR model under ambient environmental conditions (January 13, 2016) with (a) 40 ppb NO_x and 5 ppb SO_2 in the presence of 200 µg m^{-3} GDD; and (b) 40 ppb NO_x and 20 ppb SO_2 in the presence of 200 µg m^{-3} GDD. F_{water} is also predicted in each Figures. The particle loss is not considered in the simulation.

Table S1. Experimental conditions for NO_x oxidation in the presence of Gobi Desert dust (GDD) particles using an indoor chamber under different environmental conditions.

Exp. No[a]	Purpose	Type of particles	Mass conc. of particles[b] ($\mu g\ m^{-3}$) [c]	RH[c] (%)	Temp[c]. (°C)	Initial NO/NO_2 conc. (ppb) [c]	Initial O_3 conc. (ppb) [c]
GDD-1	RH effect	GDD	360.1	20.8	22.8	28.1/157.1	2.3
GDD-2	RH effect	GDD	327.5	54.8	23.1	24.1/135.1	1.6
GDD-3	RH effect	GDD	596.9	80.3	23.0	36.1/202.1	2.1
ATD-1	RH effect	ATD	433.4	20.3	23.1	25.1/140.1	1.1
ATD-2	RH effect	ATD	477.7	54.5	23.0	26.1/145.1	3.1
ATD-3	RH effect	ATD	404.9	80.1	22.0	49.1/277.1	0.7

[a] The time profile of the prediction and measurement of nitrate concentration is shown in Fig. S5.

[b] The mass concentrations of GDD particles were calculated from the SMPS data combined with the OPC data. The density of dust particles is 2.65 g cm^{-3}, and the particle size distribution was calculated up to 3 μm.

[c] The errors associated with NO, NO_2, and O_3 were ±12.5%, ±6.9%, and ±0.2%, respectively. The error associated with the dust mass were ±6% based on SMPS and OPC data. The accuracy of the RH and temperature were ±5 % and ±0.5 K, respectively.

Table S2. Summarized major chemical mechanisms for AMAR model

	Reaction	Rate constant [a]	k_1	k_2	k_3	Note[b]
			Gas-dust partitioning [c]			
1	$SO_2 + Dust \rightarrow SO_2(d) + Dust$	d	1×10^{-8}			Adams et al., 2005; Huang et al., 2015
2	$SO_2(d) \rightarrow SO_2$	e	1×10^{9}	3100	0.013	Adams et al., 2005; Huang et al., 2015
3	$O_3 + Dust \rightarrow O_3(d) + Dust$	d	1×10^{-8}			Michel et al. 2003; Underwood et al. 2001
4	$O_3(d) \rightarrow O_3$	e	3×10^{10}	2700	0	Michel et al. 2003; Underwood et al. 2001
5	$NO_2 + Dust \rightarrow NO_2(d) + Dust$	d	1×10^{-8}			Chameides 1984
6	$NO_2(d) \rightarrow NO_2$	e	1×10^{10}	2500	0	Chameides 1984
7	$HNO_3 + Dust \rightarrow HNO_3(d) + Dust$	d	1×10^{-8}			Schwartz and White 1981; Schwartz 1984
8	$HNO_3(d) \rightarrow HNO_3$	e	1×10^{15}	8700	15.4	Schwartz and White 1981; Schwartz 1984
9	$HONO + Dust \rightarrow HONO(d) + Dust$	d	1×10^{-8}			Becker et al. 1996
10	$HONO(d) \rightarrow HONO$	e	1×10^{10}	4900	0	Becker et al. 1996
11	$N_2O_5 + Dust \rightarrow HNO_3(d) + Dust$	d	7.3×10^{-3}			Wagner et al. 2009
			Dust phase			
12	$Dust + h\nu \rightarrow Dust + e\_h$		$k^{j}_{e\_h}$ [f]			this study
13	$e\_h \rightarrow energy$	g	1×10^{-2}			Yu et al. 2017
14	$e\_h + O_2 \rightarrow OH(d)$	g	$1.5\times10^{-21}\times F_{water}$			this study
15	$SO_2(d) \rightarrow SO_4^{2-}(d)$	g	5×10^{-6}			Yu et al. 2017
16	$SO_2(d) + OH(d) \rightarrow SO_4^{2-}(d)$	g	1×10^{-12}			Yu et al. 2017
17	$SO_2(d) + O_3(d) \rightarrow SO_4^{2-}(d) + O_2$	g	1×10^{-13}			Yu et al. 2017
18	$e\_h + O_3(d) \rightarrow OH(d) + O_2$	g	1×10^{-10}			Yu et al. 2017
19	$NO_2(d) \rightarrow NO_3^{-}(d)$	g	5×10^{-5}			this study
20	$e\_h + NO_2(d) \rightarrow HONO(d)$	g	6×10^{-12}			this study
21	$HONO(d) + h\nu \rightarrow OH(d) + NO$		$j_{[HONO]}$			Stockwell and Calvert, 1978; Atkinson et al., 1997

	Reaction	Rate constant [a]	k_1	k_2	k_3	Note[b]
22	$NO_2(d) + OH(d) \rightarrow NO_3^-(d)$	g	1×10^{-10}			this study
23	$NO_3^-(d) + Salt(d) \rightarrow NO_3^-(d\_salt)$	g	1×10^{-6}			this study
24	$SO_4^{2-}(d) + Salt(d) \rightarrow SO_4^{2-}(d\_salt)$	g	5×10^{-7}			this study
25	$NO_3^-(d_{salt}) + SO_4^{2-}(d) \rightarrow SO_4^{2-}(d_{salt}) + HNO_3\uparrow$	g	1×10^{-16}			this study

	Reaction	Rate constant [a]	Note[b]
		Wall loss [i]	
1	$SO_2 \rightarrow$	$(1.3RH + 3.3)\times10^{-6}$	For indoor chamber simulation; measured
2	$O_3 \rightarrow$	7×10^{-5}	For indoor chamber simulation; Chen and Jang, 2012
3	$SO_2 \rightarrow$	$(0.7RH + 1.7)\times10^{-6}$	For outdoor chamber simulation; estimated
4	$O_3 \rightarrow$	3.5×10^{-5}	For outdoor chamber simulation; estimated
5	$Dust \rightarrow$	k(dust loss)	Measured for each experiment
6	$SO_4^{2-}(aq) \rightarrow$	5×10^{-6}	Yu et al. 2017

[a] The unit of reaction rate constants is s^{-1} for first-order reactions, cm^3 molecule^{-1} s^{-1} for second-order reactions and cm^6 molecule^{-2} s^{-1} for third order reactions. The unit of the rate constants for the dust sorption reactions is m^3 m^{-2} s^{-1}.

[b] The reaction rate constants in gaseous phase, inorganic salt seeded aqueous phase and dust phase are previously reported by Yu et al. (2017). The

[c] The unit of dust for the model is mass concentration (μg m^{-3}). During simulation, the concentration of dust is multiplied by a factor of 2.45×10^{10} to have same magnitude with other gaseous species.

[d] Rate constant $k = k_1\sqrt{8\,R\,T/(\pi\,MW)}\,f_{dust,S\_M}/4$, where f_{dust,S_M} is geometric surface area normalized by dust mass (m^2 μg^{-1}), R = 8.314 is the ideal gas constant and MW is the molecule weight of chemical species.

[e] Rate constant $k = k_1 \exp\left(-\frac{k_2}{T}\right)/(F_{water}(1 + k_3/[H^+]))$, where F_{water} is calculated using Eq. (3). $[H^+]$ is the concentration of proton and is dynamically calculated using E–AIM II. (Clegg et al., 1998;Wexler and Clegg, 2002;Clegg and Wexler, 2011).

[f] The photoactivation rate contents of GDD is estimated to be 2 times higher than ATD (also see Sect 3.3).

[g] Rate constant k = k_1. The apparent rate constants are estimated semiempirically by simulating the chamber data and is only applicable to AMAR model.

[h] Rate constant k = $k_1 \exp(k_2)$.

i The wall loss factors for the model simulation are only valid for the indoor and outdoor chambers used this study. The loss factors of gases and particles may be varied for different chamber systems.

References

Clegg, S., and Wexler, A. S.: Densities and Apparent Molar Volumes of Atmospherically Important Electrolyte Solutions. 2. The Systems $H^+ - HSO_4^- - SO_4^{2-} - H_2O$ from 0 to 3 mol kg^{-1} as a Function of Temperature and $H^+ - NH_4^+ - HSO_4^- - SO_4^{2-} - H_2O$ from 0 to 6 mol kg^{-1} at 25° C Using a Pitzer Ion Interaction Model, and $NH_4HSO_4 - H_2O$ and $(NH_4)_3H(SO_4)_2 - H_2O$ over the Entire Concentration Range, J Phys Chem A, 115, 3461-3474, 2011.

Clegg, S. L., Brimblecombe, P., and Wexler, A. S.: Thermodynamic model of the system H^+-NH_4^+-SO_4^{2-}-NO_3^--H_2O at tropospheric temperatures, J Phys Chem A, 102, 2137-2154, DOI 10.1021/jp973042r, 1998.

Wexler, A. S., and Clegg, S. L.: Atmospheric aerosol models for systems including the ions H^+, NH_4^+, Na^+, SO_4^{2-}, NO_3^-, Cl^-, Br^-, and H_2O, Journal of Geophysical Research: Atmospheres, 107, 4207, 2002.

Yu, Z., Jang, M., and Park, J.: Modeling atmospheric mineral aerosol chemistry to predict heterogeneous photooxidation of SO_2, Atmos Chem Phys, 17, 10001-10017, 2017.